NASA TECHNICAL NOTE

NASA TN D-2801

NASA TN D-2801

FACILITY FORM 602

N65-23689 (ACCESSION NUMBER)

28 (PAGES)

(NASA CR OR TMX OR AD NUMBER)

(THRU) 1

(CODE) 01

(CATEGORY)

AERODYNAMIC FORCE AND MOMENT CHARACTERISTICS OF SPHERES AND CONES AT MACH 7.0 IN METHANE-AIR COMBUSTION PRODUCTS

by L. Roane Hunt

Langley Research Center

Langley Station, Hampton, Va.

GPO PRICE $ _____

CFSTI PRICE(S) $ 2.00

Hard copy (HC) _____

Microfiche (MF) $0.50

NATIONAL AERONAUTICS AND SPACE ADMINISTRATION • WASHINGTON, D. C. • MAY 1965

NASA TN D-2801

AERODYNAMIC FORCE AND MOMENT CHARACTERISTICS OF SPHERES AND CONES AT MACH 7.0 IN METHANE-AIR COMBUSTION PRODUCTS

By L. Roane Hunt

Langley Research Center
Langley Station, Hampton, Va.

NATIONAL AERONAUTICS AND SPACE ADMINISTRATION

For sale by the Clearinghouse for Federal Scientific and Technical Information
Springfield, Virginia 22151 – Price $2.00

AERODYNAMIC FORCE AND MOMENT CHARACTERISTICS OF SPHERES AND CONES AT MACH 7.0 IN METHANE-AIR COMBUSTION PRODUCTS

By L. Roane Hunt
Langley Research Center

SUMMARY

23689

An investigation has been conducted in the 7-inch Mach 7 pilot tunnel at the Langley Research Center to establish the validity of aerodynamic forces measured in a test medium composed of the combustion products of a methane-air reaction. The results, which include the drag characteristics of spheres, the longitudinal characteristics of sharp and blunt slender cones, and the center-of-pressure locations for these cones, are compared with results obtained from similar configurations tested in air and helium mediums. The data, presented in the form of aerodynamic force and moment coefficients, agree with results obtained in air and helium in both the general trend and the magnitude. Also, normal-force and pitching-moment correlation factors derived from Newtonian flow theory are found to be adequate for predicting results.

AUTHOR

INTRODUCTION

Considerable emphasis is being placed on the development of ground-test facilities which will simulate as many of the environmental conditions of hypersonic flight as possible. In many instances gases other than air are employed as the test medium to alleviate particular problems associated with the simulation. At the present time, helium and nitrogen are commonly used as test mediums in aerodynamic and fluid-mechanic ground-test facilities to avoid liquefaction and to achieve high Mach numbers. The use of methane-air combustion-products gas as a hypersonic test medium has been considered since such a gas permits a simple achievement of the proper gas energy level for flight simulation at the low end of the hypersonic speed range. The process is readily adaptable to large test facilities for which other types of energy addition systems would not be practical because of large mass-flow rate requirements.

Because the thermodynamic, transport, and flow properties of combustion products and air differ considerably, it is necessary to evaluate any differences in aerodynamic data which may result from the use of combustion products as a test medium. In reference 1 results from tests of the aerodynamic loading

and heating to hemisphere-cylinders and bluff afterbodies in such combustion products are presented and compared with results from similar investigations in which air is the test medium. The present paper presents the aerodynamic forces and moments for spheres and cones as measured in the combustion-products test medium. The tests were conducted at a stagnation temperature of about 3400° R (1890° K), a nominal Mach number of 7.0, and a stream Reynolds number per foot (per 0.305 meter) of 1×10^6 with the exception of the sphere test, for which the Reynolds number per foot was varied over a range between 0.4×10^6 and 1.5×10^6. The results are compared with results obtained from tests of similar shapes in air and helium and, where possible, with theory.

SYMBOLS

The units used for the physical quantities defined in this paper are given both in the U.S. Customary Units and in the International System of Units (SI). Factors relating the two systems are given in reference 2.

A	reference area, sq in. (sq cm)
C_A	axial-force coefficient, $\frac{\text{Axial force}}{qA}$
C_D	drag coefficient, $\frac{\text{Drag}}{qA}$
C_L	lift coefficient, $\frac{\text{Lift}}{qA}$
C_m	pitching-moment coefficient, $\frac{\text{Pitching moment}}{qA\ell}$
C_N	normal-force coefficient, $\frac{\text{Normal force}}{qA}$
d	maximum diameter of model, in. (cm)
ℓ	characteristic length, in. (cm)
L/D	lift-drag ratio
M	Mach number
R	Reynolds number
p	pressure, psia (MN/m^2)
q	free-stream dynamic pressure, psi (N/cm^2)
T	temperature, °R (°K)

x_{cp} distance along cone center line from projected cone apex to center of pressure, in. (cm)

$\bar{x}$ distance along cone center line from projected cone apex to centroid of planform area, in. (cm)

α angle of attack, deg

θ semivertex angle of cone, deg

ζ planform-area ratio, ratio of blunted-cone planform area to sharp-cone planform area

η normal-force correlating factor (eqs. (4) and (5))

ψ nose bluntness ratio, ratio of spherical nose radius to cone base radius

Subscripts:

1 condition immediately forward of normal shock

2 condition immediately behind normal shock

d maximum diameter

l characteristic length

t stagnation value

w wall value

APPARATUS AND TESTS

Models

The sphere and cone configurations used in the investigation (fig. 1) were solid (or thick wall) models constructed of type 416 stainless steel. The surface of the models was polished to a finish of approximately 16 microinches (0.406 μm) root mean square.

Sketches showing the sphere models are presented in figure 1(a). The diameters of the spheres varied from 0.50 to 1.50 inches (1.27 to 3.81 cm). Two model-support designs were employed: In one design the spheres were constructed with a stub support and in the other design the spheres were constructed with an extended support. The support length and diameter relative to the sphere diameter were varied to detect possible support interference on force measurements.

Sketches of the cone models are presented in figure 1(b). All four cones had a base diameter of 2.00 inches (5.08 cm). Three of the cones with semivertex angles of 10°, 15°, and 20° were fabricated with a sharp nose radius of 0.031 inch (0.079 cm). The fourth cone with a semivertex angle of 10° had a spherically blunted nose with a radius of 0.438 inch (1.112 cm).

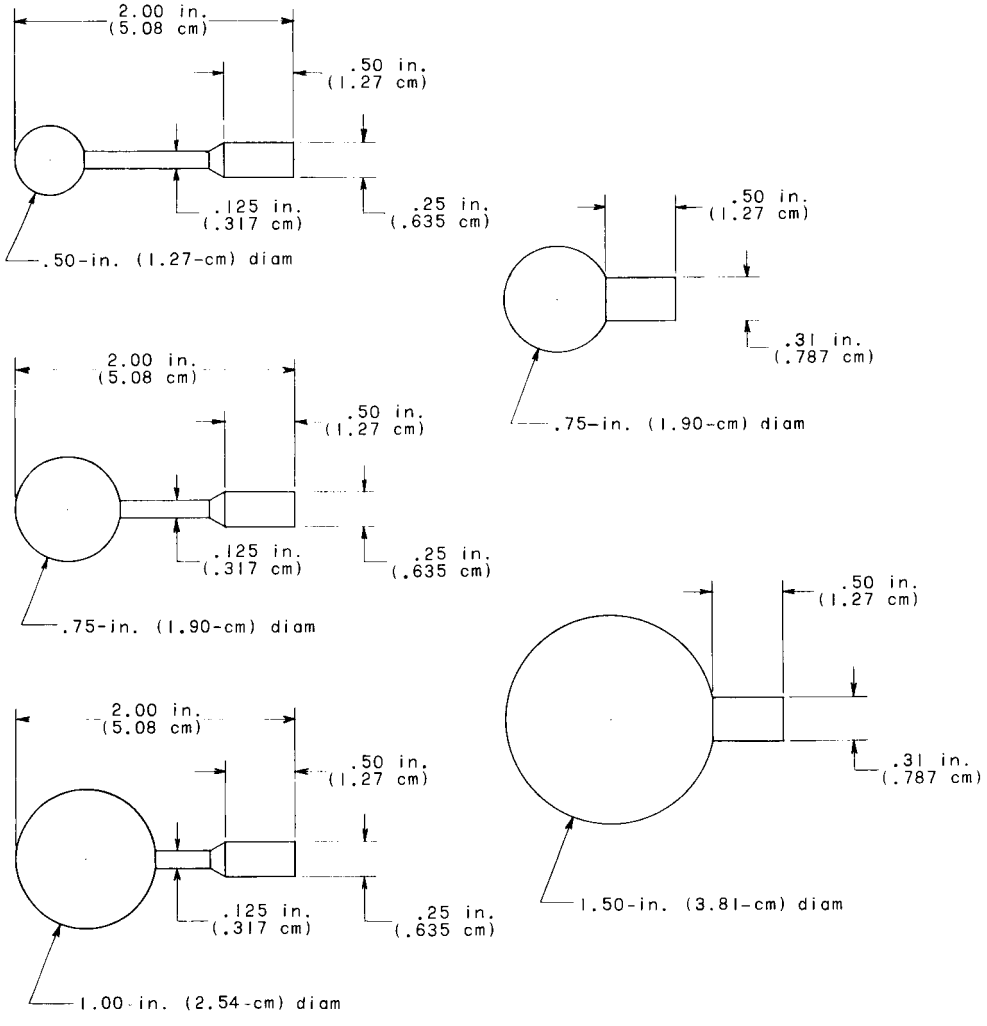

(a) Spheres.

Figure 1.- Details of models tested.

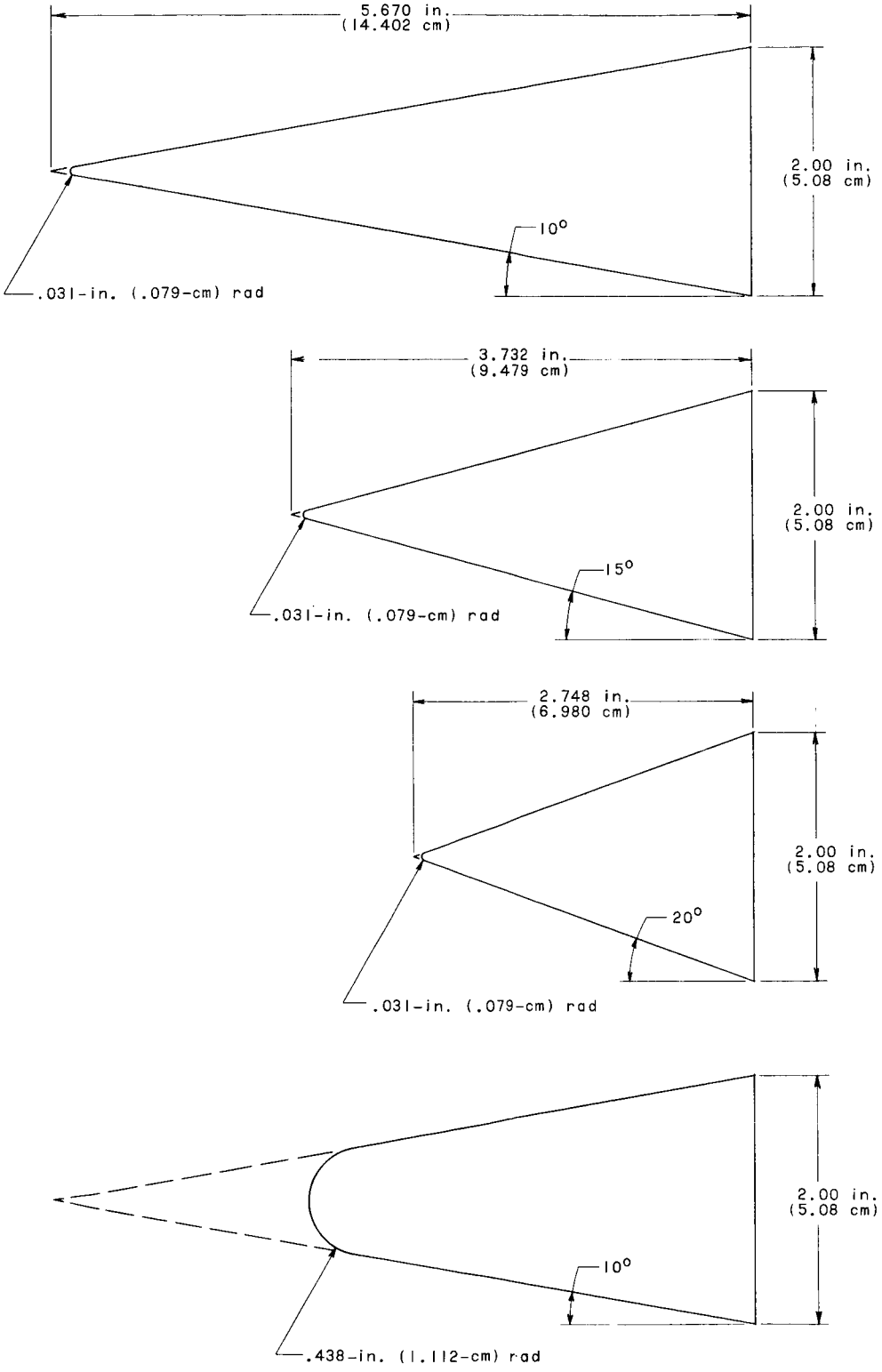

(b) Cones.

Figure 1.- Concluded.

Instrumentation

The aerodynamic forces of the models were measured with electrical strain-gage balances. The drag forces of the sphere models were indicated by the output of a single-component balance (fig. 2(a)). This balance was an external sting balance protected from the test stream by a shield. Inasmuch as the test duration required for the force measurements of the spheres was short (of the order of 6 seconds), no balance cooling was employed. Care was taken to note any posttest zero shifts which may have resulted from heat flux to the balance.

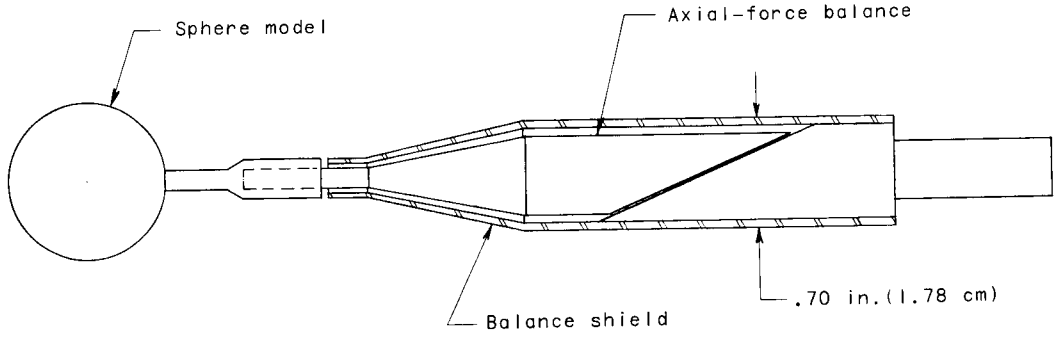

(a) Assembly for sphere.

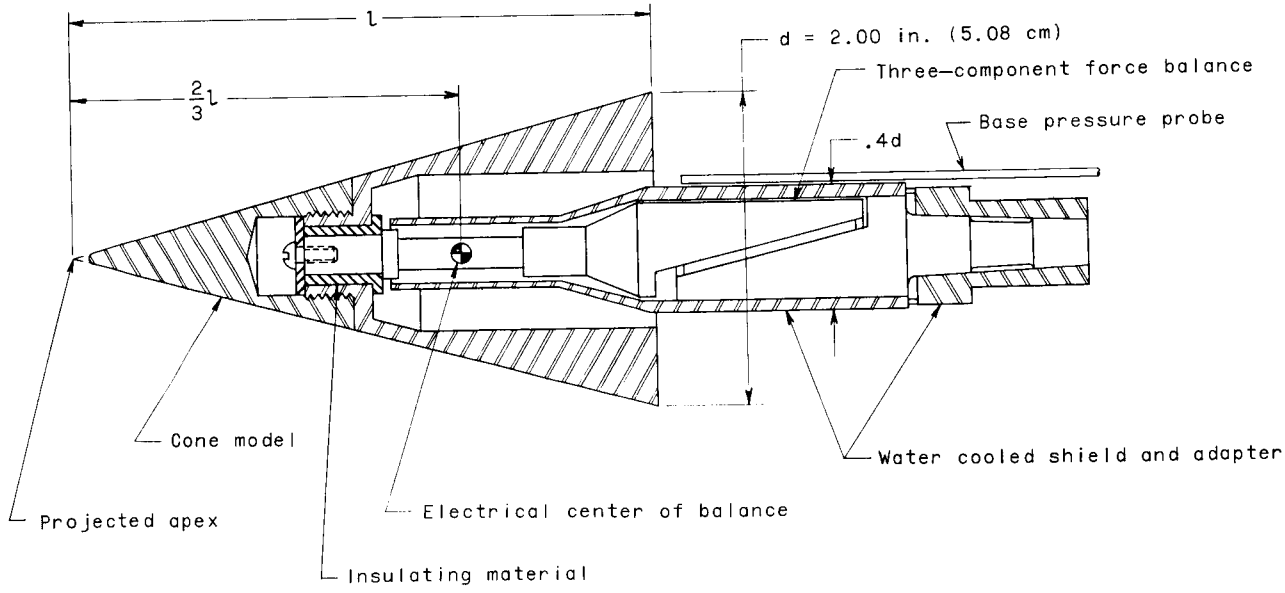

(b) Assembly for cone.

Figure 2.- Model-balance assembly.

For the cone tests a three-component force balance was used to measure the normal and axial forces and the pitching moment (fig. 2(b)). The balance shield and adapter were water cooled for these tests. In addition, spacers made of an insulating material were used to inhibit heat conduction from the model to the balance.

The base pressure of the cones was measured with a single, open-end tube positioned to face upstream and located near the cone support sting and base. (See fig. 2(b).) This pressure was indicated by the output of a pressure transducer. No base pressure measurements were made for the sphere drag tests. The outputs from the strain-gage balances, the base pressure transducer, and the tunnel reference instrumentation were recorded continuously by using either the Langley central digital data recording facility or oscillographs.

Facility

The tests were conducted in the 7-inch Mach 7 pilot tunnel at the Langley Research Center. This facility is a hypersonic blowdown tunnel with a high energy level obtained by burning a mixture of methane and air under pressure. The resulting combustion gases are expanded through a nozzle for use as the test medium. A drawing of a portion of this tunnel is shown in figure 3. Air, introduced at pressures up to 2300 psia (15.8 MN/m^2), is mixed with methane and burned in the combustion chamber. The combustion gases are then expanded to a nominal Mach number of 7.0 by use of an axisymmetric contoured nozzle. The gases flow through the free-jet test section and the straight-tube diffuser into the single-stage air ejector (not shown in the drawing) which pumps the mixture into the atmosphere. Detailed total-temperature and pitot-pressure

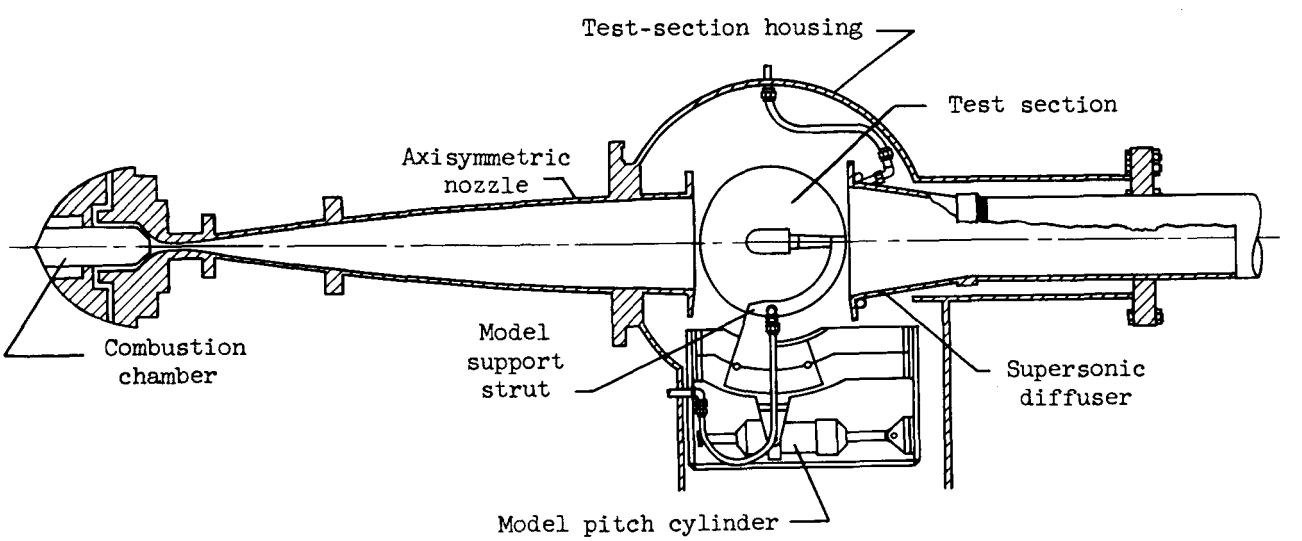

Figure 3.- Nozzle and test section of 7-inch Mach 7 pilot tunnel at the Langley Research Center.

surveys of the test region made just prior to the force tests indicate that over a core diameter of about 3 inches the total temperature and pitot pressure vary about ±2 percent. This variation corresponds to a variation in free-stream dynamic pressure of less than ±2 percent. The thermodynamic, transport, and flow properties of the gas used in the reduction of the present data are determined by the methods discussed in reference 3.

Tests

All tests were conducted at a stagnation temperature of approximately 3400° R (1890° K). The tunnel stagnation pressure was varied from 531 to 2150 psia (3.66 to 14.82 MN/m^2) in the sphere tests to provide a variation in Reynolds number, but the stagnation pressure was held constant at a nominal value of 1000 psia (6.90 MN/m^2) in the cone tests.

The general procedure was to hold the models out of the test region until the desired flow conditions were established. The model was then raised into the test position with a hydraulically operated lift which required approximately 1/4 second to position the model. The model angle of attack was predetermined and fixed. All the spheres were tested at an angle of attack of 0°. The cones, however, were tested at various angles of attack up to 20°.

Accuracy of Data

The estimated accuracies of the experimental coefficients and angle of attack are indicated in the following table (the estimates in this table correspond to an error in tunnel dynamic pressure of ±1 percent and an error in the measured forces and moments of ±1 percent of balance-rated loads):

Sphere drag coefficient	±0.02
Cone normal-force coefficient	±0.01
Cone axial-force coefficient	±0.01
Cone pitching-moment coefficient	±0.01
Angle of attack, deg	±0.1

RESULTS AND DISCUSSION

The data were reduced to the conventional coefficients C_N, C_A, C_m, C_L, and C_D. The reference area used in deriving the coefficient values was the maximum cross-sectional area for the spheres and the area defined by $l^2 \tan \theta$ for the cones. In this expression, l is the characteristic length (fig. 2(b)) and θ is the cone semivertex angle. The pitching-moment coefficients are referenced to the projected apex of the cone.

Sphere Drag

The test conditions and experimental results from the sphere tests are presented in table I. Included in the table are the tunnel stagnation temperature and pressure, the stream Mach number, the Reynolds number forward and behind the normal portion of the bow shock in front of the spheres, and the drag coefficient.

TABLE I.- PERTINENT DATA FROM DRAG TEST OF SPHERES

Run	T_t		$P_{t,1}$		M_1	$R_{d,1}$	$R_{d,2}$	C_D
	°R	°K	psia	MN/m²				
d = 0.50 in. (1.27 cm)								
1	3660	2033	549	3.78	6.89	1.59×10^4	3.46×10^3	0.941
2	3510	1950	954	6.58	6.97	2.59	5.39	.937
3	3400	1889	923	6.36	7.01	2.82	5.78	.960
4	3320	1844	1437	9.91	7.10	4.39	8.80	.933
5	3550	1972	2150	14.82	7.09	5.94	10.9	.958
d = 0.75 in. (1.905 cm)								
6	3480	1933	549	3.78	6.96	2.56×10^4	5.35×10^3	0.967
7	3470	1928	923	6.36	7.00	4.13	8.31	.931
8	3470	1928	1435	9.89	7.04	6.10	12.3	.927
9	3440	1911	2140	14.75	7.13	9.06	18.2	.937
d = 0.75 in. (1.905 cm)*								
10	3560	1978	549	3.78	6.91	2.51×10^4	5.37×10^3	0.957
11	3480	1933	1425	9.83	7.04	6.13	12.3	.925
d = 1.00 in. (2.54 cm)								
12	3490	1939	549	3.78	6.96	3.34×10^4	6.95×10^3	0.938
13	3660	2033	934	6.44	6.91	5.18	10.9	.933
14	3630	2017	938	6.47	6.93	5.18	10.9	.944
15	3630	2017	1448	9.98	6.98	7.94	16.8	.931
16	3520	1955	2140	14.75	7.11	1.17	24.4	.961
d = 1.50 in. (3.81 cm)*								
17	3460	1922	531	3.66	6.97	4.99×10^4	10.3×10^3	0.957
18	3575	1985	934	6.44	6.96	7.85	16.8	.950
19	3630	2017	1445	9.96	7.04	11.7	24.6	.933

*Stub support.

A comparison of the drag coefficients of the present test with the results obtained from tests in air (refs. 4 to 8) is presented in figure 4. The drag-coefficient results taken from the references are plotted as a function of Mach number. The drag coefficient obtained from the modified Newtonian theory is also presented. For the flow conditions for which the Reynolds number is large, the variation of sphere drag coefficient with Mach number is fairly well defined by the data from references 4, 5, and 6. Between Mach numbers 4 and 10 the drag coefficient is essentially independent of Mach number, as indicated by the data from reference 6. In general, the present data are in fair agreement with the data obtained from tests in air. However, the present drag-coefficient data and those of reference 8 are slightly higher than both the general level of the other experimental data and the theoretical value. The higher drag-coefficient values for the data of reference 8 are attributed to low Reynolds number effects. Inasmuch as the Reynolds numbers for the present tests are considerably lower than those for references 4, 5, and 6, low Reynolds number effects are assumed to account for the higher drag coefficients obtained in the present tests.

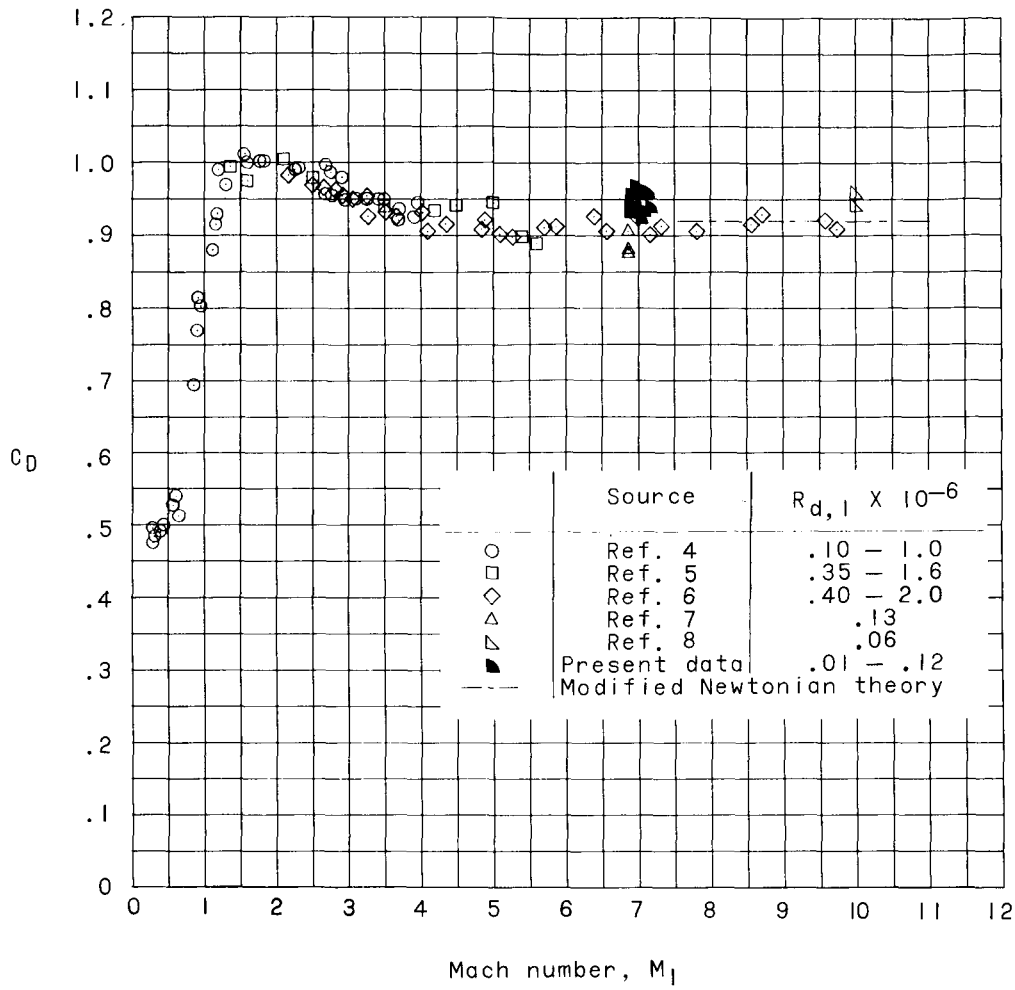

Figure 4.- Variation of sphere drag coefficient with Mach number from numerous nonviscous ballistic and wind-tunnel tests.

In order to examine the Reynolds number effects on the sphere drag, the present data are plotted in figure 5 as a function of the Reynolds number based on conditions immediately behind the normal shock. The three curves in this figure are empirically determined curves from reference 8, which in turn were based on the experimental results of references 6, 8, and 9, together with other experimental results. These curves represent the variation of the sphere drag coefficient with Reynolds number for three wall-temperature ratios. Hypersonic data from references 6, 7, and 8 as well as the low Reynolds number results for ratios of wall temperature to stagnation temperature of 1.00 and 0.26 from reference 9 are plotted in figure 5. For flow in which $R_{d,2}$ is less than 10^5, the drag coefficient increases with an increase in the ratio of wall temperature to stagnation temperature and with a decrease in Reynolds number. When compared on the basis of Reynolds number, the present data are in good agreement with the empirical curves. The results plotted in figures 4 and 5 indicate that any effect of support interference on the drag data is negligible for the present tests.

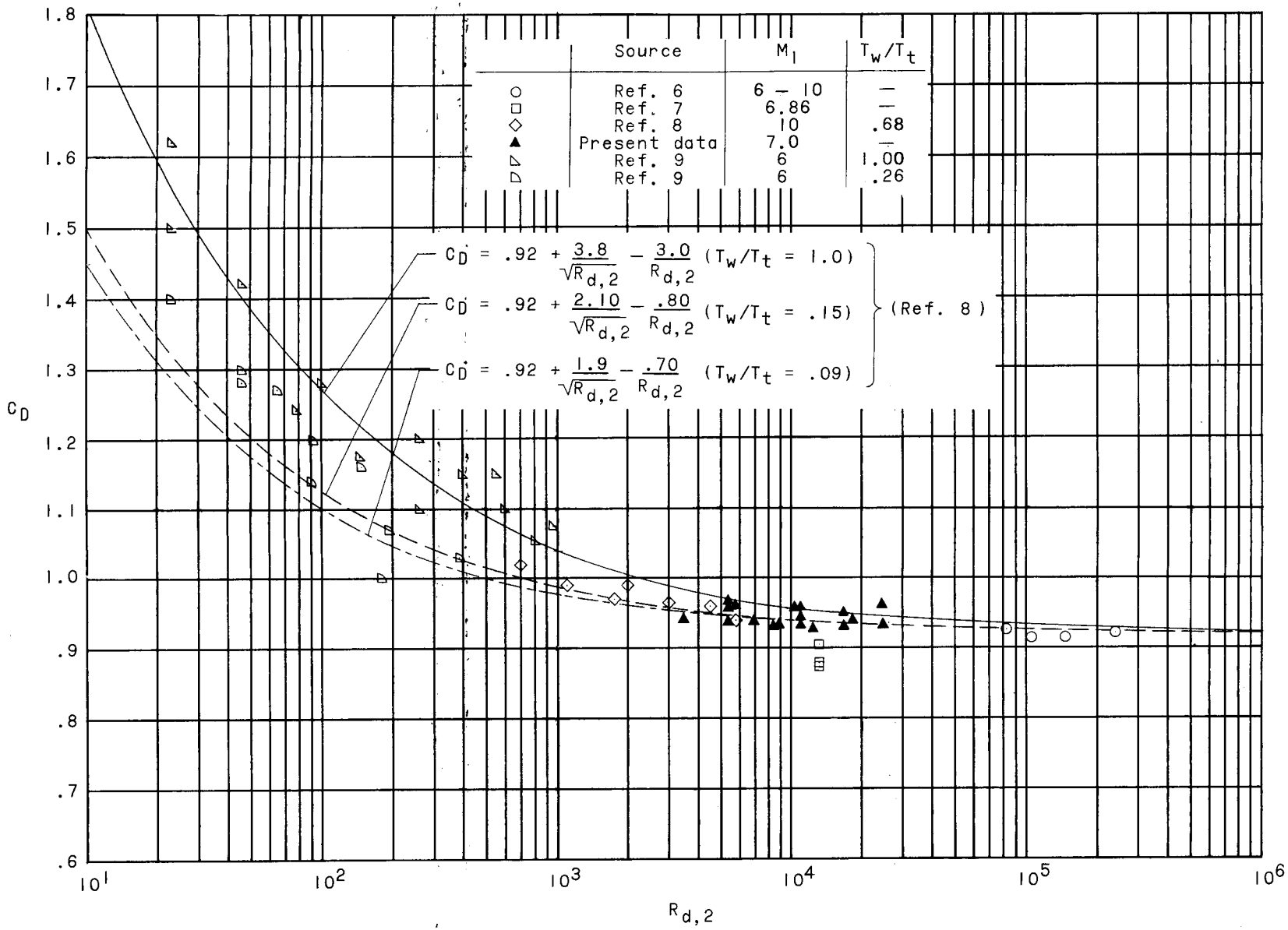

Figure 5.- Variation of sphere drag coefficient with Reynolds number for wall-temperature ratios at hypersonic Mach numbers.

Cone Forces and Moments

The data obtained from the force tests of the cones are tabulated and presented in table II. Included in this table are the cone angles of attack, the tunnel stagnation conditions, and the stream Reynolds number based on the cone characteristic length for each test run. Also tabulated are values of C_N, C_A, C_m, C_L, C_D, and L/D.

TABLE II.- PERTINENT DATA FROM FORCE TESTS OF CONES

Run	α, deg	T_t		$p_{t,l}$		$R_{l,l}$	C_N	C_A	C_m	C_L	C_D	L/D
		°R	°K	psia	MN/m²							
θ = 10°, l = 5.67 in. (14.4 cm), ψ = 0.031												
1	0.50	3200	1778	1018	7.02	4.54×10^5	0.00887	0.0529	-0.00630	0.0084	0.0530	0.159
2	5.25	3310	1839	1022	7.05	4.28	.0970	.0589	-.0664	.0912	.0675	1.350
3	9.96	3210	1783	1022	7.05	4.54	.1867	.0701	-.1280	.1718	.1013	1.695
4	15.15	3235	1797	1022	7.05	4.49	.2897	.0854	-.1976	.2573	.1582	1.626
5	20.33	3370	1872	1019	7.03	4.20	.3961	.1054	-.2688	.3348	.2365	1.416
θ = 15°, l = 3.73 in. (9.47 cm), ψ = 0.031												
6	0.50	3420	1900	1028	7.09	2.72×10^5	0.0152	0.1478	-0.0115	0.0139	0.1480	0.0937
7	5.63	3385	1880	1021	7.04	2.72	.1473	.1544	-.1052	.1315	.1681	.782
8	10.00	3435	1908	1027	7.08	2.70	.2669	.1663	-.1902	.2339	.2101	1.114
9	15.17	3360	1867	1033	7.12	2.78	.3990	.1879	-.2828	.3360	.2857	1.176
10	20.25	3410	1894	1025	7.07	2.70	.5312	.2189	-.3772	.4226	.3892	1.086
θ = 20°, l = 2.75 in. (6.98 cm), ψ = 0.031												
11	0.33	3385	1880	1016	7.01	2.01×10^5	0.0118	0.3201	-0.0099	0.0099	0.3201	0.0310
12	.33	3360	1867	1027	7.08	2.03	.0095	.3222	-.0074	.0077	.3222	.0236
13	.60	3260	1811	1032	7.12	2.17	.0164	.3260	-.0247	.0129	.3266	.0396
14	5.67	3385	1880	1024	7.06	2.01	.1941	.3240	-.1467	.1612	.3416	.4718
15	10.00	3460	1922	1022	7.05	1.95	.3372	.3294	-.2545	.2749	.3830	.7180
16	15.02	3435	1908	1028	7.09	2.01	.5019	.3519	-.3773	.3933	.4699	.8370
17	20.33	3410	1894	1022	7.05	2.01	.6512	.3864	-.4887	.4764	.5885	.8093
θ = 10°, l = 5.67 in. (14.4 cm), ψ = 0.438												
18	0.50	3260	1811	1026	7.07	4.40×10^5	0.00216	0.1328	-0.0019	0.0010	0.1328	0.0076
19	5.25	3310	1839	1025	7.07	4.28	.0576	.1348	-.0426	.0451	.1395	.3232
20	9.96	3260	1811	1023	7.05	4.40	.1191	.1431	-.0888	.0926	.1615	.5732
21	15.15	3260	1811	1017	7.01	4.40	.2177	.1569	-.1652	.1691	.2083	.8117
22	20.33	3270	1817	1019	7.03	4.40	.3244	.1741	-.2446	.2437	.2754	.8849

The force and moment coefficients and the lift-drag ratio for the sharp nose cones with 10°, 15°, and 20° semivertex angles are plotted as a function of angle of attack in figure 6. Also plotted in figure 6 are the results from references 10, 11, and 12, obtained from tests in air and helium. The dashed curves in the figure represent results from Newtonian theory plotted from the tabulated values of reference 13. As can be seen, the normal-force coefficients (fig. 6(a)), the pitching-moment coefficients (fig. 6(c)), and the lift coefficients (fig. 6(d)) obtained from tests in combustion products, air, and helium agree within experimental accuracy among themselves, and they also agree with the Newtonian theory. The axial-force coefficients (fig. 6(b)) and drag coefficients (fig. 6(e)) also agree for the various test mediums; however, the Newtonian theory prediction is below the experimental results primarily because of viscous effects. In order to include the viscous drag effects in the theoretical prediction, skin-friction coefficients computed by the reference temperature method as outlined in reference 14 are used. Newtonian theory modified to include viscous effects is represented by the solid curves in figures 6(b) and 6(e) for angles of attack near 0°. As would be expected, the theoretical prediction and experimental results are in closer agreement when viscous effects are included.

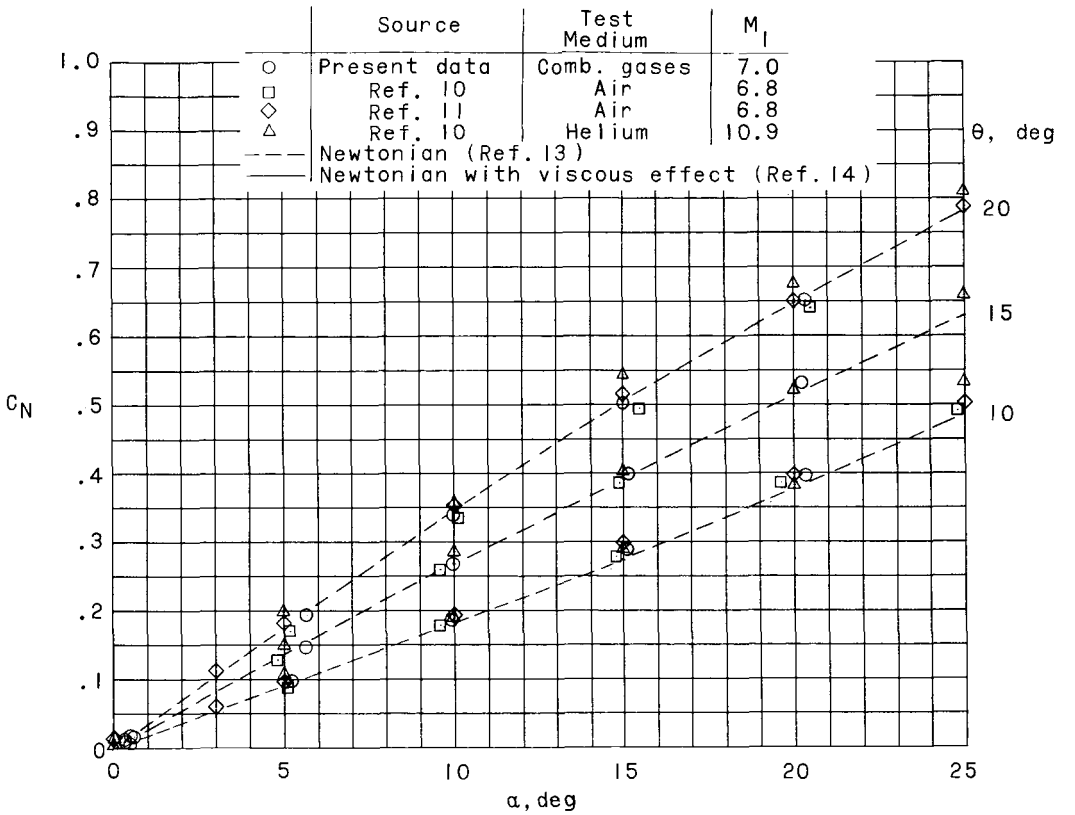

(a) Normal-force coefficient.

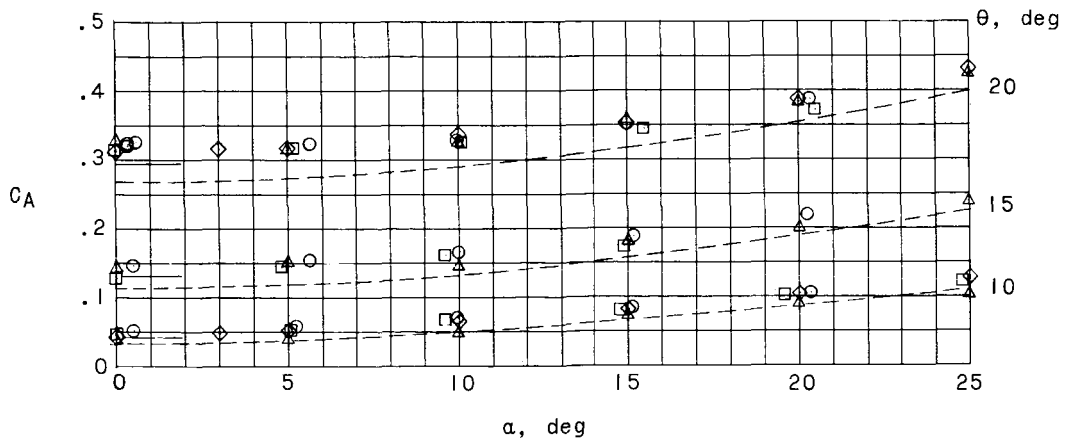

(b) Axial-force coefficient.

Figure 6.- Variation of force and moment coefficients and lift-drag ratio with angle of attack for sharp nose cones of semivertex angles of 10^0, 15^0, and 20^0.

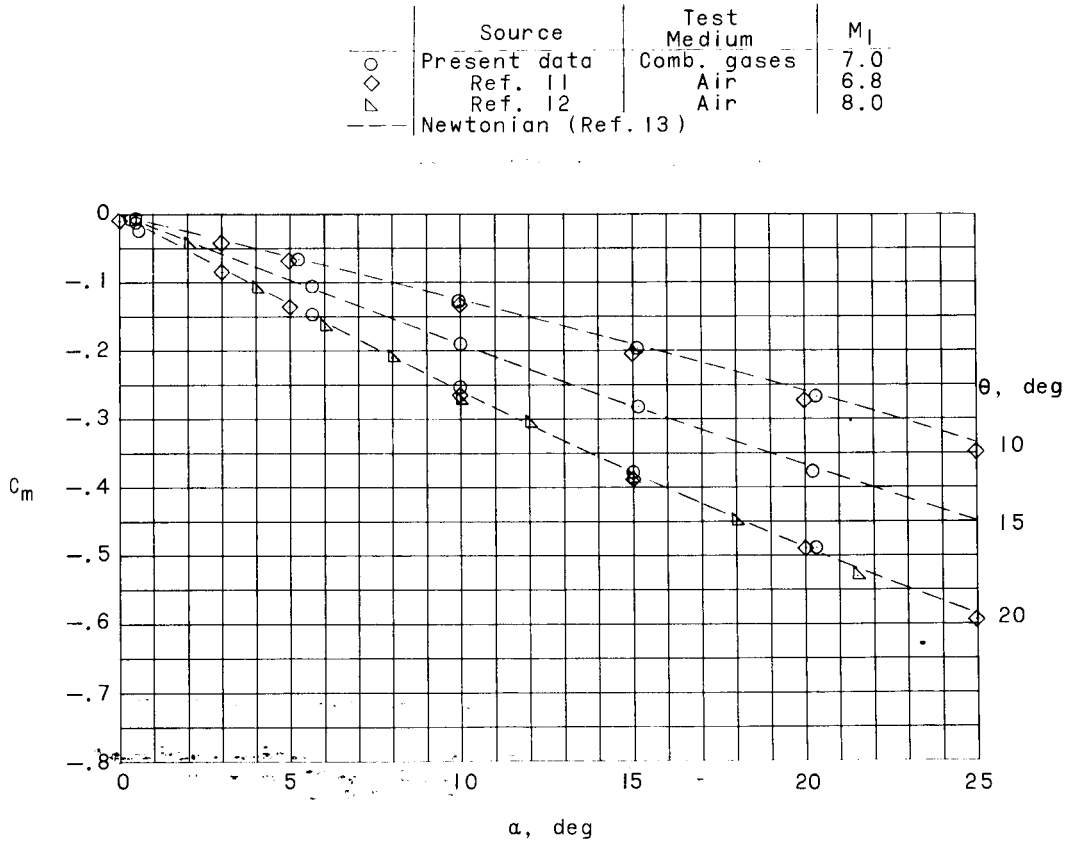

(c) Pitching-moment coefficient.

Figure 6.- Continued.

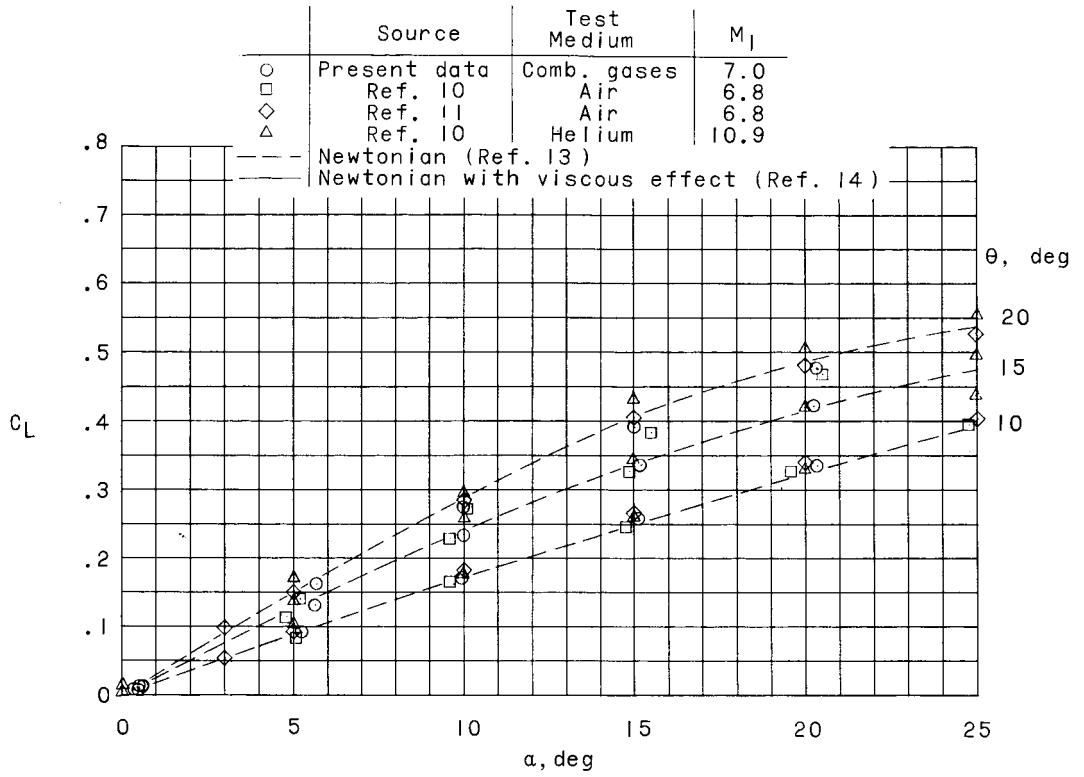

(d) Lift coefficient.

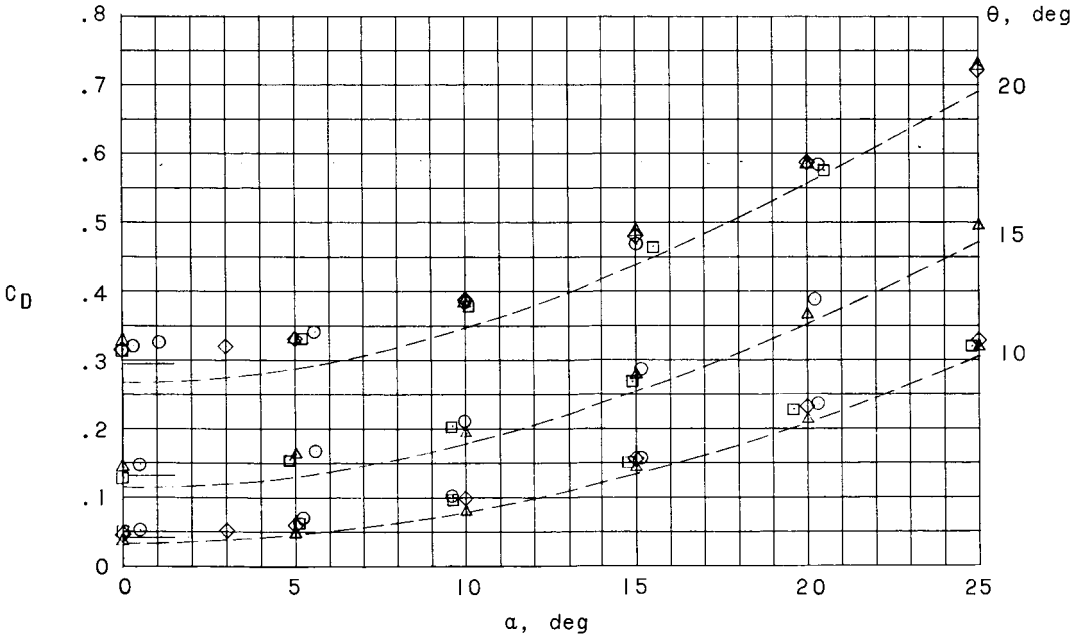

(e) Drag coefficient.

Figure 6.- Continued.

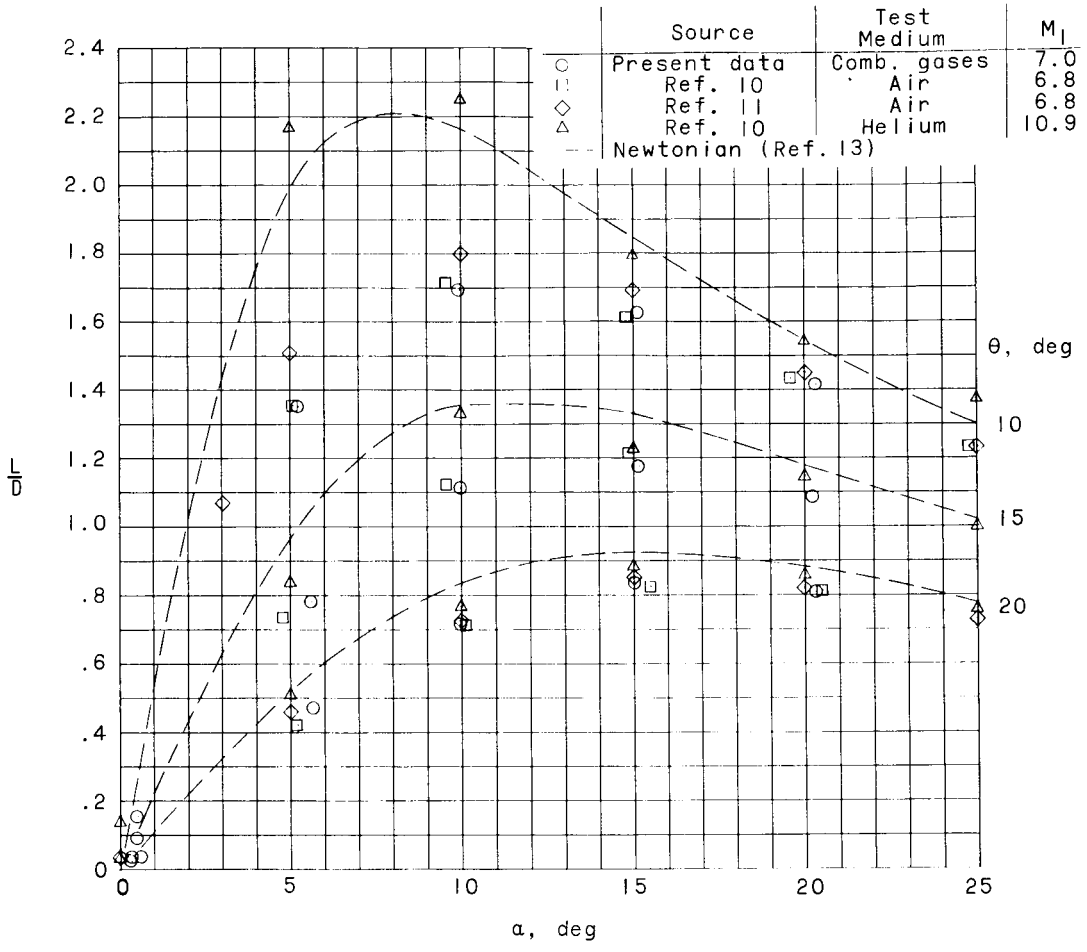

(f) Lift-drag ratio.

Figure 6.- Concluded.

The results obtained from tests of the blunt and sharp 10° cones in the combustion-products medium are compared with other results obtained from tests of similar configurations in air and are presented in figure 7 as a function of cone bluntness for several angles of attack. The solid curves are the results of reference 15 cross-plotted to give a comparison at each angle of attack. Sharp-cone results of reference 10, which were obtained from tests in air, are also presented in figure 7. The normal-force-coefficient, pitching-moment-coefficient, and lift-coefficient comparisons shown in figures 7(a), 7(c), and 7(d), respectively, indicate very good agreement between present results and the results of reference 15. The axial-force-coefficient and drag-coefficient comparisons in figures 7(b) and 7(e) also indicate good agreement, although, in general, the data of reference 15 are slightly higher than both the present results and the results of reference 10. The present results and the results of references 10 and 15 were obtained from tests having the same general Reynolds number level.

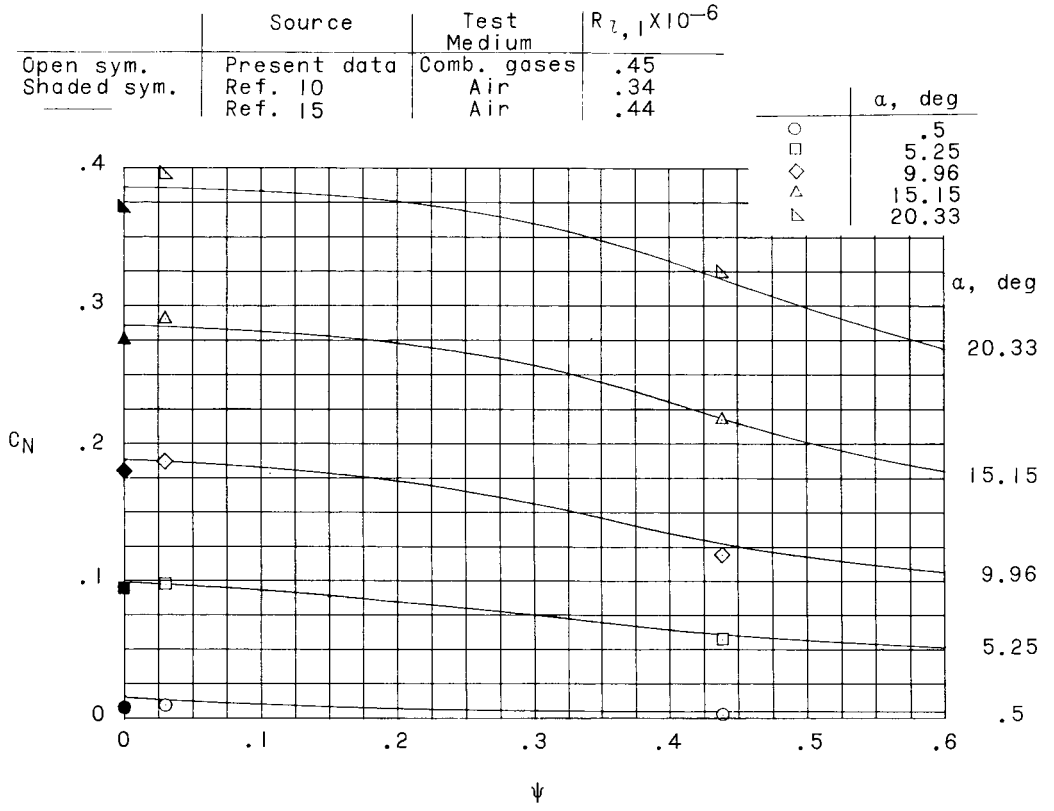

(a) Normal-force coefficient.

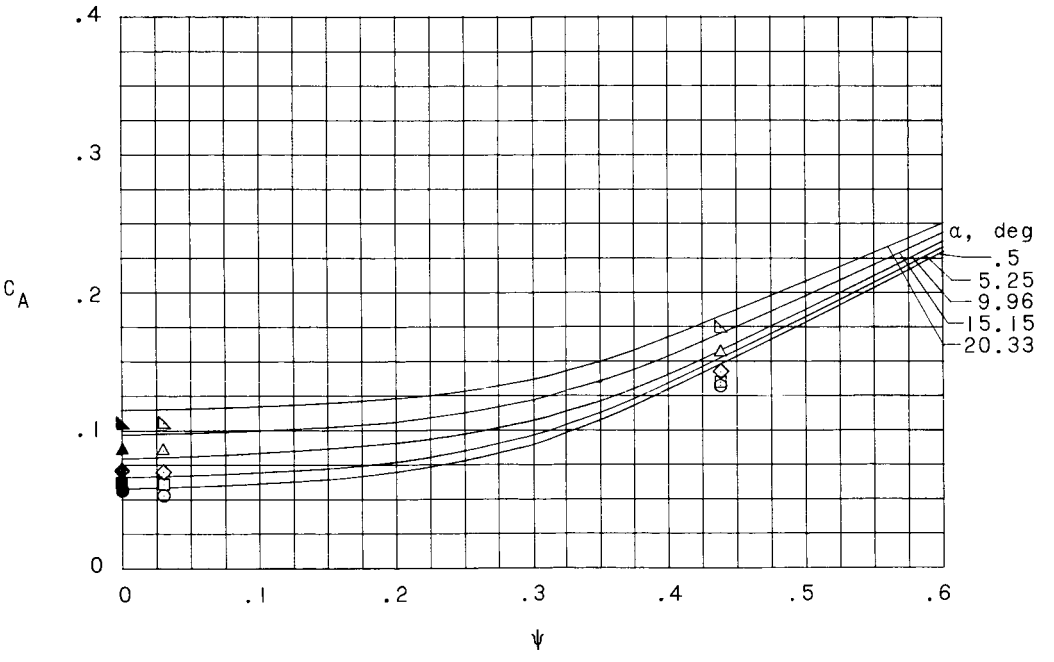

(b) Axial-force coefficient.

Figure 7.- Variation of force and moment coefficients with nose bluntness for 10^0 semivertex angle cones at angles of attack ranging from 0.5^0 to 20.33^0.

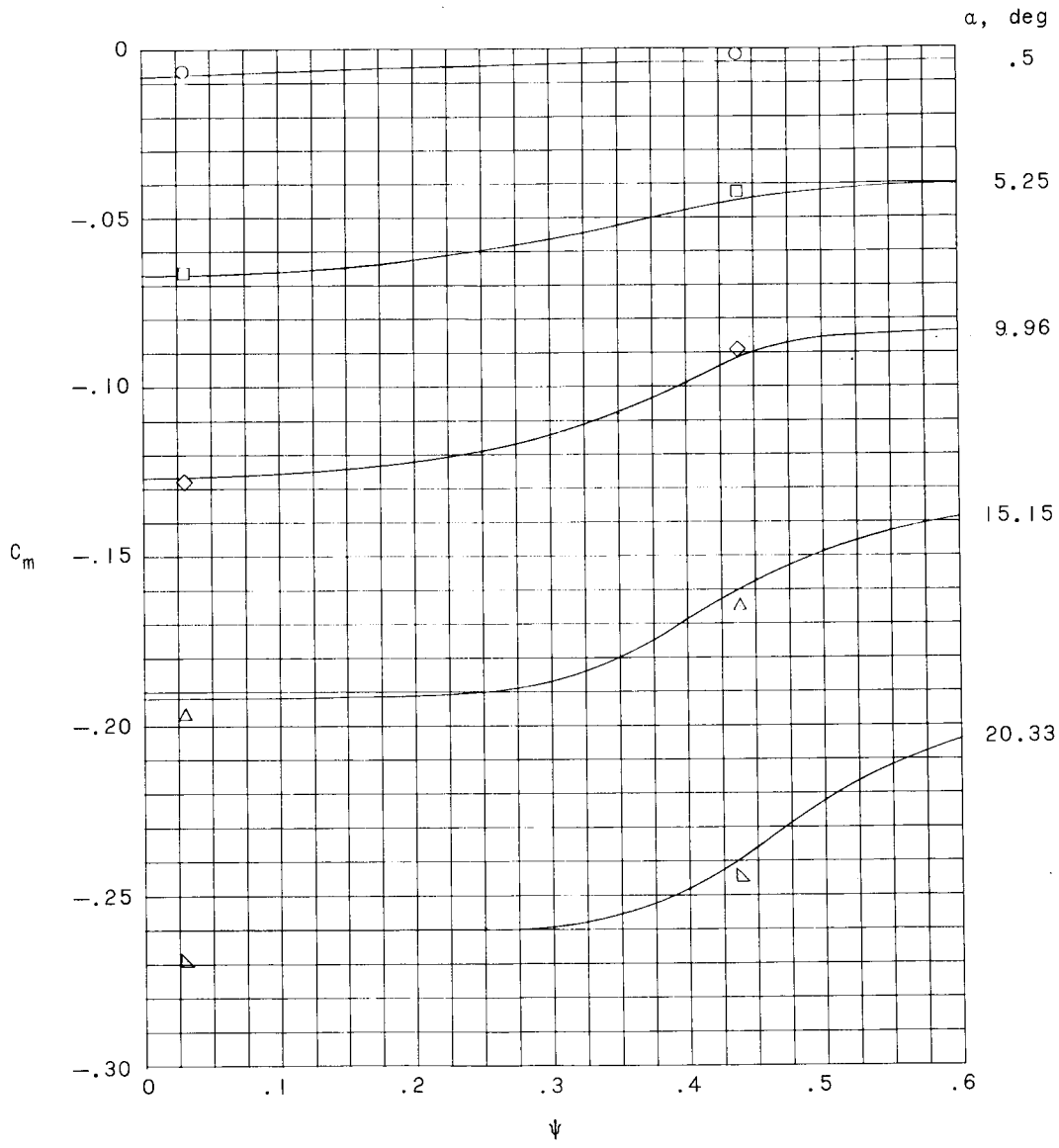

(c) Pitching-moment coefficient.

Figure 7.- Continued.

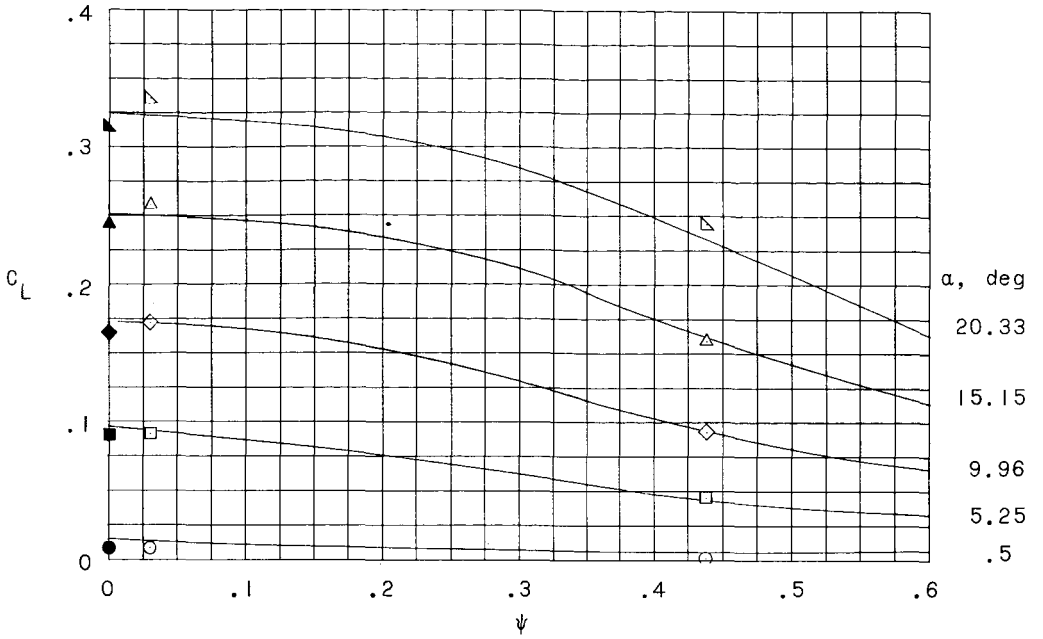

(d) Lift coefficient.

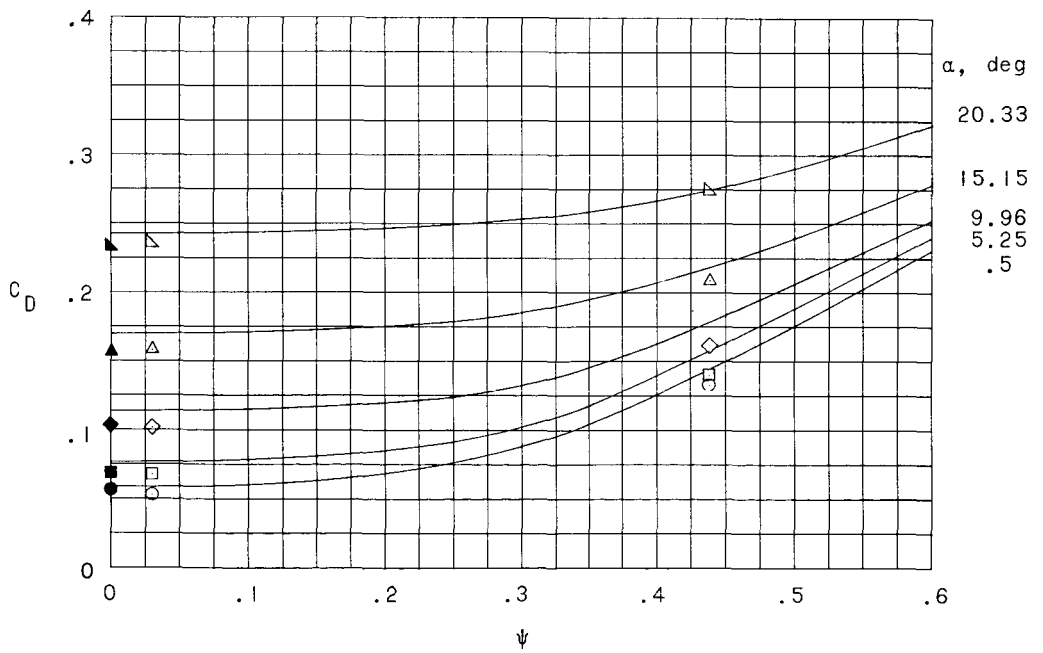

(e) Drag coefficient.

Figure 7.- Concluded.

Normal-force correlation.- An attempt was made to correlate the normal-force results of the present tests with results of other references by using an analysis similar to that suggested in reference 16. In the analysis of reference 16, Newtonian theory is used to correlate the normal-force coefficient in terms of the angle of attack, the semivertex angle, and the degree of spherical bluntness of the cone. This analysis involves restrictive assumptions which make it inapplicable to the present tests. The present analysis is also based on Newtonian theory; however, in this paper, the normal-force coefficient is assumed to be proportional to the sine squared of the local flow angle along the windward side of the cone. Therefore, the normal-force coefficient which accounts for only the windward normal force can be expressed by the relation

$$C_N \propto \zeta \sin^2(\theta + \alpha) \tag{1}$$

In this relation, ζ is the planform-area ratio which is used to adjust the normal-force coefficient to the proper reference area as defined previously. An expression for the normal-force coefficient which accounts for only the leeward normal force is obtained in the same manner as that used to obtain relation (1). Combining the windward normal force and the leeward normal force yields

$$C_N \propto \zeta \left[\sin^2(\theta + \alpha) - \sin^2(\theta - \alpha)\right] \tag{2}$$

Relation (2) can be reduced to

$$C_N \propto \zeta \sin 2\theta \sin 2\alpha \tag{3}$$

In using relations (1) and (3), the leeward normal-force component is assumed to be negligible when the cone angle of attack is greater than the cone semivertex angle. The correlating factor η is defined as follows:

For $\alpha \leqq \theta$

$$\eta = \zeta \sin 2\theta \sin 2\alpha \tag{4}$$

and for $\alpha \geqq \theta$

$$\eta = \zeta \sin^2(\theta + \alpha) \tag{5}$$

The normal-force results from the present tests and those from references 12, 15, and 17 are presented as a function of η in figure 8. The curve in this figure is derived from the Newtonian theory (ref. 13) and indicates that the normal-force coefficient is linear with η. As can be seen, the correlation is very good, particularly for the results from sharp-cone tests.

The results from blunt-cone tests fall below the Newtonian prediction; thus the leeward normal-force component acting on the spherically blunted nose is probably underestimated in the present analysis. A linear empirical equation which defines C_N as a function of cone semivertex angle, nose bluntness, and angle of attack is derived from figure 8 and is as follows:

$$C_N = 1.57\eta \tag{6}$$

In general, the correlation of the normal-force results is good and the present results agree with the results obtained in air.

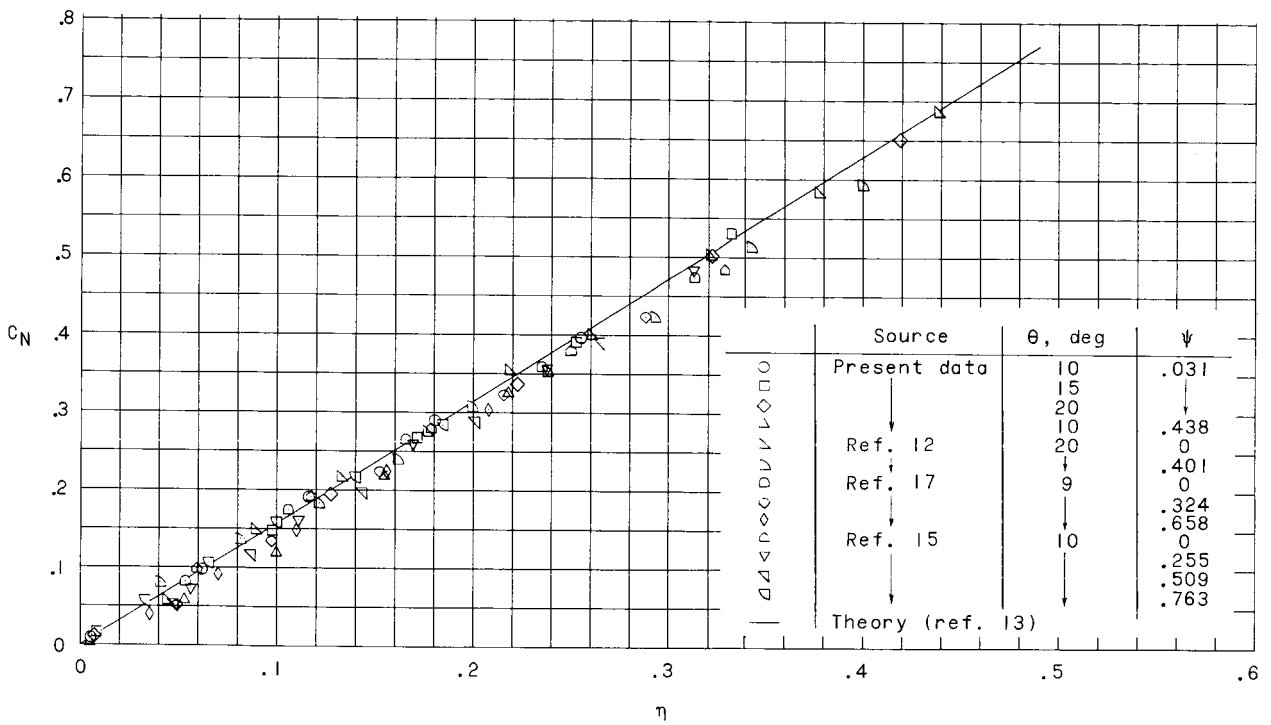

Figure 8.- Normal-force correlation with two relations derived from Newtonian theory for sharp and blunt cones.

Cone center of pressure.- Knowledge of the location of the center of pressure is helpful in correlating pitching-moment data with normal-force data. The pitching-moment coefficient is equal to the product of the normal-force coefficient and the center-of-pressure distance parameter; that is,

$$C_m = C_N \frac{x_{cp}}{l} \tag{7}$$

For sharp cones, the location x_{cp} is defined by Newtonian theory as

$$\frac{x_{cp}}{l} = \frac{2}{3}\sec^2\theta \tag{8}$$

where x_{cp} is independent of angle of attack but dependent on the cone semivertex angle. (See discussion of center-of-pressure location in refs. 11 and 13.) For the evaluation of the center-of-pressure locations for the present cones, the value 2/3 in equation (8) is replaced by the geometric centroid parameter. Equation (8) becomes

$$\frac{x_{cp}}{l} = \frac{\overline{x}}{l} \sec^2\theta \tag{9}$$

The center-of-pressure locations for sharp cones are plotted as a function of angle of attack in figure 9. The present data agree with the experimental data of reference 11 (solid symbols) and with Newtonian theory (eq. (9)). The experimental data support the prediction of equation (9) that the center of pressure is independent of the cone angle of attack. Similar trends are also noted for the blunt cone. (See fig. 10.)

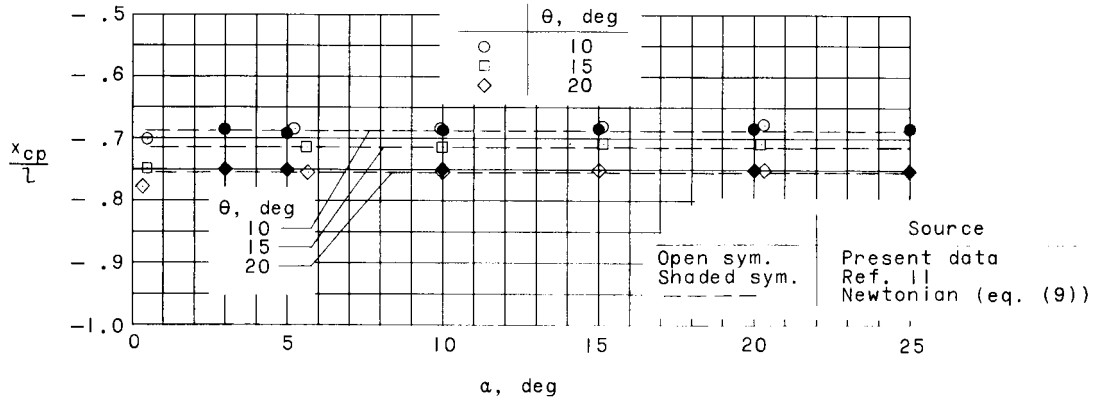

Figure 9.- Variation of center-of-pressure location with angle of attack for sharp nose cones with semivertex angles of 10^0, 15^0, and 20^0.

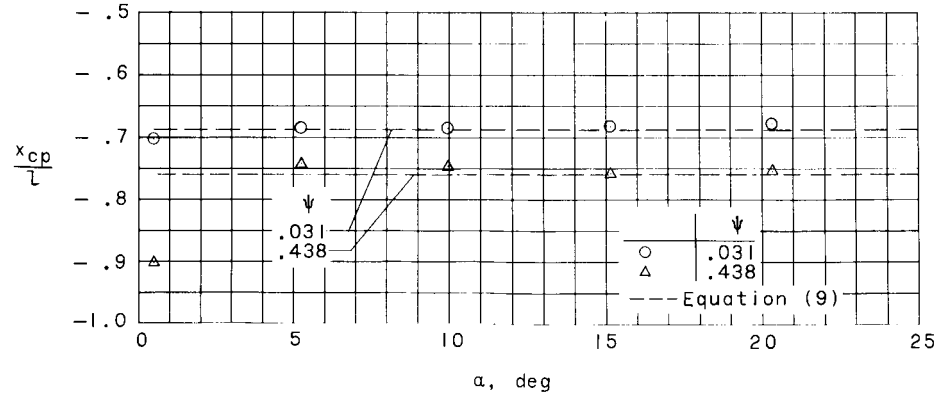

Figure 10.- Variation of center-of-pressure location with angle of attack for cones with semivertex angle of 10^0 and two nose bluntness ratios.

In order to correlate the pitching-moment coefficient with the normal-force coefficient, the following equation, which is obtained from equations (7) and (9), was used:

$$C_m = C_N \frac{\bar{x}}{l} \sec^2\theta \tag{10}$$

The correlation is presented in figure 11. The results for cones of various semivertex angles and nose bluntnesses obtained from the present tests and from references 12 and 15 are shown. As can be seen in figures 9, 10, and 11, the center-of-pressure locations for cones tested in both combustion-products and air test mediums agree and are accurately predicted by theory.

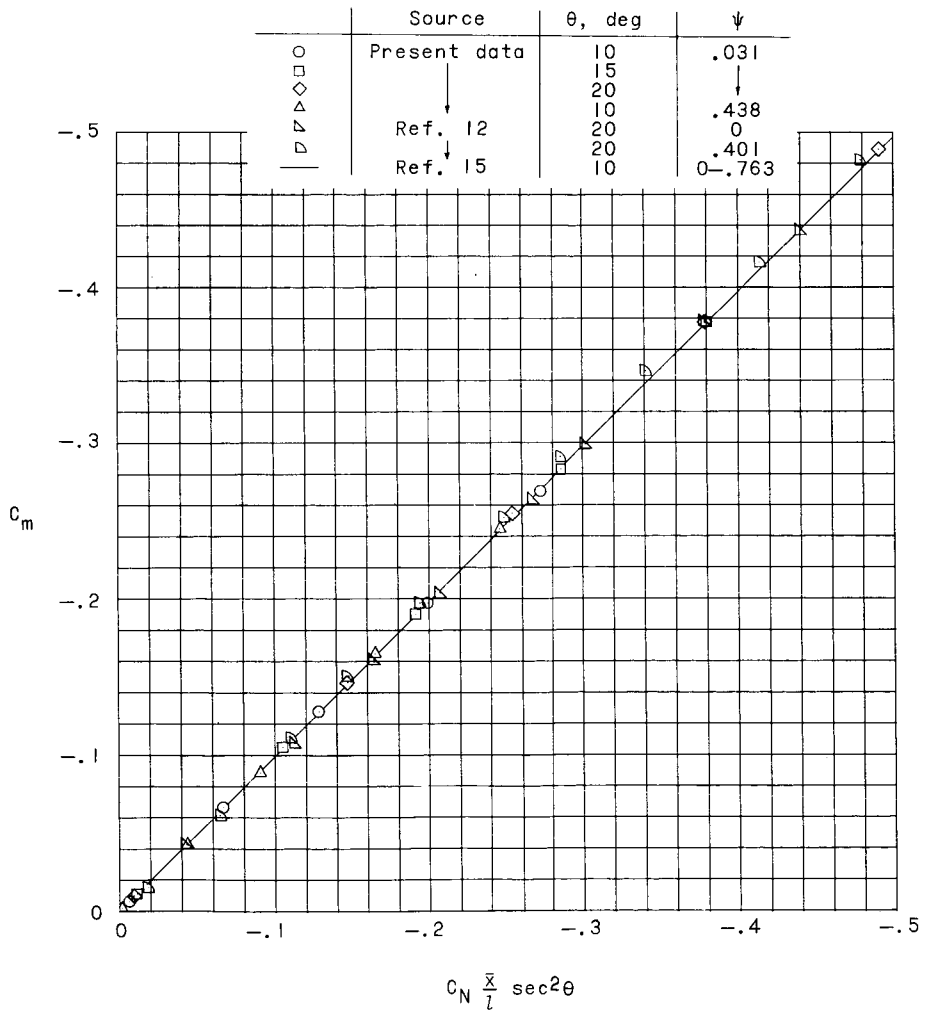

Figure 11.- Correlation of pitching moment with product of normal force and nondimensional distance from center-of-pressure location to projected apex for sharp and blunt cones.

CONCLUDING REMARKS

Aerodynamic force tests in which the combustion products of a methane-air reaction is used as the test medium have been conducted on spheres and cones in the 7-inch Mach 7 pilot tunnel at the Langley Research Center. The results of the tests are compared with results obtained from tests of similar models in air and helium test mediums and, where possible, with theory. The comparisons made include the drag characteristics of spheres, the longitudinal characteristics of sharp and blunt slender cones, and the center-of-pressure locations for these cones.

In general, the nondimensionalized coefficients computed from measurements obtained in the combustion-products test medium agreed well with results previously obtained in air and helium test mediums. The sphere drag coefficients obtained in the combustion gases agreed with those values determined in other experimental studies which considered both the pressure and viscous effects. The present results for the sharp nose cone agreed with results obtained from similar models tested in air, and they were adequately predicted by Newtonian theory with the exception of the axial-force and the drag coefficients. For these two coefficients, account had to be taken of viscous effects before acceptable agreement with theory could be achieved. The present experimental results presented for the blunt cone also agreed with other previously obtained experimental results. The center-of-pressure locations for the cones obtained from the present tests agreed with those calculated from Newtonian theory and with those obtained from previous tests in air. Also, normal-force and pitching-moment coefficients for all cone semivertex angles and degrees of nose bluntness presented were successfully correlated by use of Newtonian theory.

Langley Research Center,
National Aeronautics and Space Administration,
Langley Station, Hampton, Va., February 16, 1965.

REFERENCES

1. Weinstein, Irving: Heat Transfer and Pressure Distributions on a Hemisphere-Cylinder and a Bluff-Afterbody Model in Methane-Air Combustion Products and in Air. NASA TN D-1503, 1962.

2. Mechtly, E. A.: The International System of Units - Physical Constants and Conversion Factors. NASA SP-7012, 1964.

3. Leyhe, E. W.; and Howell, R. R.: Calculation Procedure for Thermodynamic, Transport, and Flow Properties of the Combustion Products of a Hydrocarbon Fuel Mixture Burned in Air With Results for Ethylene-Air and Methane-Air Mixtures. NASA TN D-914, 1962.

4. Charters, A. C.; and Thomas, R. N.: The Aerodynamic Performance of Small Spheres From Subsonic to High Supersonic Velocities. Jour. Aero. Sci., vol. 12, no. 4, Oct. 1945, pp. 468-476.

5. Clark, A. B. J.; and Harris, Fred T. (With appendix by R. E. Roberson): Free-Flight Air-Drag Measurement Techniques. NRL Rep. 3727, Naval Res. Lab., Sept. 6, 1950.

6. Hodges, A. J.: The Drag Coefficient of Very High Velocity Spheres. Jour. Aero. Sci., vol. 24, no. 10, Oct. 1957, pp. 755-758.

7. Penland, Jim A.: Aerodynamic Characteristics of a Circular Cylinder at Mach Number 6.86 and Angles of Attack up to 90°. NACA TN 3861, 1957. (Supersedes NACA RM L54A14.)

8. Kinslow, Max; and Potter, J. Leith: The Drag of Spheres in Rarefied Hypervelocity Flow. AEDC-TDR-62-205, U.S. Air Force, Dec. 1962.

9. Aroesty, Jerome: Sphere Drag in a Low Density Supersonic Flow. Rept. No. HE-150-192 (Contract N-onr-222(45)), Inst. Eng. Res., Univ. of California, Jan. 3, 1962.

10. Ladson, Charles L.; and Blackstock, Thomas A. (With appendix by Donald L. Baradell and Thomas A. Blackstock): Air-Helium Simulation of the Aerodynamic Force Coefficients of Cones at Hypersonic Speeds. NASA TN D-1473, 1962.

11. Penland, Jim A.: A Study of the Stability and Location of the Center of Pressure on Sharp, Right Circular Cones at Hypersonic Speeds. NASA TN D-2283, 1964.

12. Merz, G. H.; and Pritts, O. R.: Static Force Tests at Mach 8 of Sharp and Blunt 20-Deg Half-Angle Cones and a Blunt 70-Deg Swept Delta Wing. AEDC-TDR-62-187, U.S. Air Force, Oct. 1962.

13. Wells, William R.; and Armstrong, William O.: Tables of Aerodynamic Coefficients Obtained From Developed Newtonian Expressions for Complete and Partial Conic and Spheric Bodies at Combined Angles of Attack and Sideslip With Some Comparisons With Hypersonic Experimental Data. NASA TR R-127, 1962.

14. Francis, W. Leon; Malvestuto, Frank S., Jr.; and Stuart, Jay W., Jr.: Study To Determine Skin-Friction Drag in Hypersonic Low-Density Flow - Vol. I: Summary Analysis. Tech. Rept. No. ASD-TR-61-433, vol. I, U.S. Air Force, Apr. 1962.

15. Harris, Julius E.: A Basic Study of Spherically Blunted Cones Including Force and Moment Coefficient Correlation and Air-Helium Simulation Studies. M.S. Thesis, Virginia Polytechnic Inst., 1964.

16. Whitfield, Jack D.; and Wolny, W.: Hypersonic Static Stability of Blunt Slender Cones. AEDC-TDR-62-166 (Contract No. AF 40(600)-1000), Arnold Eng. Dev. Center, Aug. 1962.

17. Neal, Luther, Jr.: Aerodynamic Characteristic at a Mach Number of 6.77 of a 9° Cone Configuration, With and Without Spherical Afterbodies, at Angles of Attack up to 180° With Various Degrees of Nose Blunting. NASA TN D-1606, 1963.

NASA-Langley, 1965 L-4248